Directed spiral site percolation on the square lattice

S.B. Santra[a]

Department of Physics, Indian Institute of Technology Guwahati, Guwahati-781039, Assam, India

Abstract. A new site percolation model, directed spiral percolation (DSP), under both directional and rotational (spiral) constraints is studied numerically on the square lattice. The critical percolation threshold $p_c \approx 0.655$ is found between the directed and spiral percolation thresholds. Infinite percolation clusters are fractals of dimension $d_f \approx 1.733$. The clusters generated are anisotropic. Due to the rotational constraint, the cluster growth is deviated from that expected due to the directional constraint. Connectivity lengths, one along the elongation of the cluster and the other perpendicular to it, diverge as $p \to p_c$ with different critical exponents. The clusters are less anisotropic than the directed percolation clusters. Different moments of the cluster size distribution $P_s(p)$ show power law behaviour with $|p - p_c|$ in the critical regime with appropriate critical exponents. The values of the critical exponents are estimated and found to be very different from those obtained in other percolation models. The proposed DSP model thus belongs to a new universality class. A scaling theory has been developed for the cluster related quantities. The critical exponents satisfy the scaling relations including the hyperscaling which is violated in directed percolation. A reasonable data collapse is observed in favour of the assumed scaling function form of $P_s(p)$. The results obtained are in good agreement with other model calculations.

PACS. 64.60.-i General studies of phase transitions – 83.80.Gv Electro- and magnetorheological fluids – 72.80.Tm Composite materials

1 Introduction

Recently, there is strong interest in studying properties of electro-rheological and magneto-rheological fluids [1], magnetic semiconductors [2], and composite materials [3] because of their industrial applications. A new site percolation model, directed spiral percolation (DSP), proposed here could be applied in general to study their rheological, electrical and magnetic properties. The DSP model is constructed imposing both directional and rotational constraints on the ordinary percolation (OP) model [4]. The directional constraint is in a fixed direction in space and the empty sites in that direction are accessible to occupation. Due to the rotational constraint the sites in the forward direction or in a rotational direction, say clockwise, are accessible to occupation. The direction of the rotational constraint is not fixed in space and it depends on the direction from which the present site is occupied. For charged particles, the directional constraint in the model could arise from an electric field along a particular direction in the plane of the lattice and the rotational constraint may arise from a magnetic field applied perpendicular to the plane. The model will also be applicable to the physical situations corresponding to the presence of other kinds of directional and rotational constraints.

The effect of two different external constraints, directional constraint and rotational (spiral) constraint, on the ordinary percolation model have been studied independently. The corresponding models are known as directed percolation (DP) model [5] and spiral percolation (SP) model [6]. The DP model has applications in self-organized criticality [7], reaction diffusion systems [8], nonlinear random resistor networks [9] etc. The SP model has been applied in studying spiral forest fire [10], pinning of interfaces [11], and diffusion under rotational bias in disordered systems [12]. It is observed that in the presence of an external constraint the critical properties of the system as well as the universality class of the OP model are changed [13]. The critical exponents associated with different cluster related quantities in the DP and SP models are not only different but also different from those in the case of the OP model. The DP and SP models then belong to two different universality classes than that of the OP model.

In this paper, the proposed DSP model is studied numerically on the square lattice in two dimensions ($2D$). The external constraints in the model determine the nearest empty sites available for occupation. A single cluster growth Monte Carlo (MC) algorithm is developed for this model under both the external constraints. Critical percolation probability p_c, at which a spanning (or infinite) cluster appears for the first time, is determined. The spanning clusters are found fractals. The clusters generated in the OP and the SP models are isotropic. In DP, the clusters are anisotropic and elongated along the directional constraint. The clusters generated in the case of the DSP
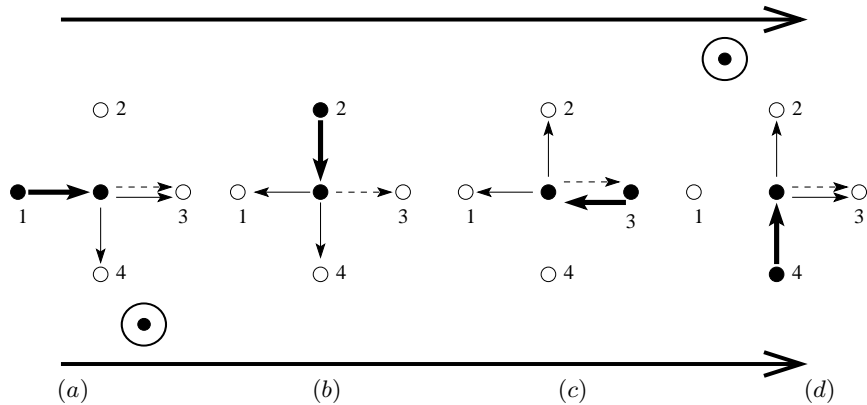
[a] e-mail: santra@iitg.ernet.in

Fig. 1. Selection of empty nearest neighbors of an occupied site for occupation. Black circles are the occupied sites and open circles are the empty sites. Two thick long arrows from left to right represent the directional constraint. The presence of clockwise rotational constraint is shown by the encircled dots. The eligible empty nearest neighbors of the central occupied site will be selected here for occupation. The direction from which the central site is occupied is indicated by a short thick arrow. The dotted arrow indicates the sites allowed by the directional constraint and the thin arrows indicate the sites allowed by the rotational constraint. In (a), the central site is occupied from the left and the sites 3 and 4 are accessible to occupation. In (b), the central site is approached from the top and sites 1, 3 and 4 could be occupied. In (c), the central site is occupied from the right and 1, 2, and 3 are probable for occupation. Notice that the site 3, already an occupied site, could be reoccupied from a different direction. In (d), the central site is approached from the below and sites 2 and 3 are the probable sites for occupation.

model are anisotropic but they grow in a direction different from the directional constraint due to the presence of the rotational constraint. A new type of cluster is thus generated in this model. The connectivity length exponents $\nu_\parallel$ and $\nu_\perp$ are estimated. $\nu_\parallel$ is approximately equal to the connectivity exponent ν of OP but both $\nu_\parallel$ and $\nu_\perp$ are different from those obtained in DP. The clusters are less anisotropic than DP clusters. Different moments of the cluster size distribution $P_s(p)$ become singular as $p \to p_c$ with their respective critical exponents. The values of the critical exponents obtained here are different from those obtained in other percolation models like OP, DP, and SP. The DSP model then belongs to a new universality class. A scaling theory is developed. The critical exponents satisfy the scaling relations within error bars including the hyperscaling which is violated in DP. A reasonable data collapse is observed in support of the assumed scaling function form of $P_s(p)$. The results obtained in this model are in good agreement with the results obtained in the study of magnetoresistance in a model of 3-constituents composite material [14].

2 The DSP model

A square lattice of size $L \times L$ is considered. A directional constraint from left to right and a clockwise rotational constraint are imposed on the system. Due to the directional constraint any empty site on the right of an occupied site could be occupied in the next Monte Carlo (MC) time step. Due to the rotational constraint the empty sites in the forward direction or in the clockwise direction can be occupied. To generate clusters under these two constraints a single cluster growth algorithm is developed following the original algorithm of Leath [15]. In this algorithm, the central site of the lattice is occupied

with unit probability. All four nearest neighbors to the central site can be occupied with equal probability p in the first time step. As soon as a site is occupied, the direction from which it is occupied is assigned to it. In the next MC time step, two empty sites due to the rotational constraint and the site on the right due to the directional constraint will be eligible for occupation for each occupied site in the previous time step. This is illustrated in Figure 1. The directional constraint is represented by two long arrows from left to right. The presence of the rotational constraint is shown by the encircled dots. The black circles represent the occupied sites and the open circles represent the empty sites. The empty nearest neighbors of the central occupied site will be selected for occupation in this step. The direction from which the central site is occupied is represented by a short thick arrow. The dotted arrow indicates the eligible empty site for occupation due to directional constraint and the thin arrows indicate the eligible empty sites for occupation due to the rotational constraint. Since the directional constraint is to the right, site 3, an empty site on the right of the occupied site, is always eligible for occupation. The sites accessible to occupation due to the rotational constraint will be identified now. The rotational constraint acts in the forward or in the clockwise direction and depends on the direction of approach to the present occupied site. In Figure 1a, the central site is occupied from site 1 on the left. Thus, site 3 in the forward direction and site 4 in the clockwise direction are the eligible sites for occupation due to the rotational constraint. In this situation, sites 3 and 4 are then the only eligible sites for occupation in the next time step due to both the constraints. In Figure 1b, the central site is occupied from site 2 on the top and thus, sites 4 and 1 are the eligible sites for occupation due to the rotational constraint. The available sites for occupation are 1, 3 and 4 due to both the constraints in this case. In

Figure 1c, the eligible sites for occupation are 1 and 2 due to the rotational constraint and site 3 due to the directional constraint. Note that, site 3 is already an occupied site and could be reoccupied from a different direction. A site is forbidden for occupation from the same direction. On the square lattice, a site then could be occupied at most 4 times from 4 possible directions. This is unlike the case of the ordinary and directed percolations where a site is occupied only once. In Figure 1d, sites 2 and 3 are eligible for occupation due to both the constraints. It can be seen that the direction of the rotational constraint is not fixed in space and depends on the previous time step whereas that of the directional constraint remains fixed in space. In that sense, the directional constraint is a global constraint and the rotational constraint is a local constraint in the model. After selecting the eligible sites for occupation, they are occupied with probability p. The coordinate of an occupied site in a cluster is denoted by (x,y). Periodic boundary conditions are applied in both directions and the coordinates of the occupied sites are adjusted accordingly whenever the boundary is crossed. At each time step the span of the cluster in the x and y directions $L_x = x_{max} - x_{min}$ and $L_y = y_{max} - y_{min}$ are determined. If L_x or $L_y \geq L$, the system size, then the cluster is considered to be a spanning cluster. The critical percolation probability p_c is defined as below which there is no spanning cluster and at $p = p_c$ a spanning cluster appears for the first time in the system.

A typical spanning or infinite cluster generated on a 128×128 square lattice at $p = 0.655$ is shown in Figure 2. The black dots represent the occupied sites. The cross near to the upper left corner is the origin of the cluster (it was the central site of the lattice). The thick arrows from left to right at the top and bottom represent the directional constraint. The encircled points in the upper right and lower left corners represent the existence of the clockwise rotational constraint. Notice that all the dangling ends are clockwisely turned as it is expected. The cluster is highly rarefied. Holes of all possible sizes are there. The elongation of the cluster is almost along the left upper to the right lower diagonal of the lattice and not along the directional constraint applied in the x direction. The geometry of the infinite clusters in other percolation models are the following. In OP, the clusters are isotropic. In DP, the anisotropic clusters are elongated along the applied field [16]. In SP, the clusters are compact and isotropic [17]. Not only the geometry but also the internal structure, highly rarefied with curly dangling ends, of the cluster is different from that of the infinite clusters in other percolation models. A new type of anisotropic cluster is thus generated in the DSP model.

3 Scaling theory

The cluster related quantities and their singularities at $p = p_c$ are defined here. Scaling relations among the critical exponents describing the singularities of the cluster related quantities will also be established. The cluster

Fig. 2. An infinite cluster on a 128×128 square lattice at $p = 0.655$ is shown. The black dots are the occupied sites. The cross on the upper left corner is the origin of the cluster. The thick arrows on the top and bottom from left to right represent directional constraint. The presence of the clockwise rotational constraint is shown by the encircled dots. The cluster is highly rarefied and has holes of almost all possible sizes. The elongation of the cluster is along the upper left to the lower right diagonal and not along the directional constraint. The dangling ends are clockwisely rotated.

size distribution is defined as

$$P_s(p) = \frac{N_s}{N_{tot}} \tag{1}$$

where N_s is the number of s-sited clusters in a total of N_{tot} clusters generated. In the single cluster growth method, the origin is occupied with unit probability. The scaling function form of the cluster size distribution is then assumed to be

$$P_s(p) = s^{-\tau+1}\mathsf{f}[s^{\sigma}(p - p_c)] \tag{2}$$

where τ and σ are two exponents.

The order parameter of the percolation transition is the probability that a site belongs to a spanning (or infinite) cluster and here it is defined as $P_\infty = p - p\sum'_s P_s(p)$. The sum is over all the finite clusters and it is indicated by a prime. The leading singularity of P_∞ will be governed by $\sum'_s P_s(p)$, the zeroth moment of cluster size distribution.

P_∞ goes to zero as $p \to p_c$ from the above with a critical exponent β. The exponent β is defined as

$$P_\infty \sim (p - p_c)^\beta. \tag{3}$$

An important cluster related quantity is the average cluster size χ. In the single cluster growth method it is the first moment of the cluster size distribution $P_s(p)$ and defined as $\chi = \sum'_s sP_s(p)$ where the sum is over the finite clusters. Two next higher moments χ_1 and χ_2 are also defined as $\chi_1 = \sum'_s s^2 P_s(p)$ and $\chi_2 = \sum'_s s^3 P_s(p)$. In the present context these higher moments have no physical meaning but might be useful in particular situations. The moments χ, χ_1, and χ_2 diverge with their respective critical exponent γ, δ, and η at $p = p_c$. The critical exponents γ, δ, and η are defined as

$$\chi \sim |p - p_c|^{-\gamma}, \ \ \chi_1 \sim |p - p_c|^{-\delta}, \ \ \ \chi_2 \sim |p - p_c|^{-\eta}. \tag{4}$$

Since the cluster related quantities are just different moments of the cluster size distribution function $P_s(p)$ then the critical exponents associated with them are not all independent. All the critical exponents could be expressed in terms of the exponents τ and σ needed to describe $P_s(p)$ (Eq. (2)). It could be shown that the kth moment of $P_s(p)$ become singular as

$$\Sigma'_s s^k P_s(p) \sim (p - p_c)^{-(k - \tau + 2)/\sigma}. \tag{5}$$

Putting the value of k, the order of the moment, in equation (5) one could obtain the following scaling relations

$$\beta = (\tau - 2)/\sigma, \quad \gamma = (3 - \tau)/\sigma, \quad \delta = (4 - \tau)/\sigma,$$
$$\text{and} \quad \eta = (5 - \tau)/\sigma. \tag{6}$$

Eliminating τ and σ, scaling relations between β, γ, δ, and η could be obtained as

$$\delta = \beta + 2\gamma, \qquad \eta = 2\delta - \gamma. \tag{7}$$

Since the clusters generated here are anisotropic in nature, two lengths, $\xi_\parallel$ and $\xi_\perp$, are needed to describe the connectivity of the occupied sites. $\xi_\parallel$ is the connectivity length along the elongation of the cluster and $\xi_\perp$ is the connectivity length along the perpendicular direction to the elongation. To measure $\xi_\parallel$ and $\xi_\perp$ the moment of inertia tensor $\mathbf{T}$, a 2×2 matrix here, is calculated. For a s-sited cluster, the xy component of the tensor is given by

$$T_{xy} = \sum_{\ell=1}^{s} (x_\ell - x_0)(y_\ell - y_0) \tag{8}$$

where x_ℓ and y_ℓ are the x and y coordinates of the ℓth site and (x_0, y_0) is the coordinate of the center of mass of the cluster. The radii of gyration $R_\parallel(s)$ and $R_\perp(s)$ with respect to two principal axes could be obtained as $R_\parallel^2(s) = \lambda_1/s$ and $R_\perp^2(s) = \lambda_2/s$ where λ_1 is the largest eigenvalue and λ_2 is the smallest eigenvalue of the 2×2 moment of inertia matrix $\mathbf{T}$. $R_\perp$ is about the axis passing through (x_0, y_0) and along the elongation of the cluster

and $R_\parallel$ is about the axis perpendicular to the elongation and passing through (x_0, y_0). The connectivity lengths now can be determined as

$$\xi_\parallel^2 = \frac{2\sum'_s R_\parallel^2(s)sP_s(p)}{\sum'_s sP_s(p)}, \quad \text{and} \quad \xi_\perp^2 = \frac{2\sum'_s R_\perp^2(s)sP_s(p)}{\sum'_s sP_s(p)}. \tag{9}$$

The correlation lengths $\xi_\parallel$ and $\xi_\perp$ diverge with two different critical exponents $\nu_\parallel$ and $\nu_\perp$ as $p \to p_c$. The critical exponents $\nu_\parallel$ and $\nu_\perp$ are defined as

$$\xi_\parallel \sim |p - p_c|^{-\nu_\parallel}, \qquad \xi_\perp \sim |p - p_c|^{-\nu_\perp}. \tag{10}$$

The cluster mass is given by the number of sites s in the cluster and is expected to scale as $s \approx R_\parallel R_\perp^{(d_f - 1)}$ at $p = p_c$, and it should go as $s \approx R_\parallel R_\perp^{(d-1)}$ above p_c, where d is the spatial dimension of the lattice and d_f is the fractal dimension of the infinite clusters generated on the same lattice. The percolation probability P_∞ is the ratio of the number of sites on the infinite cluster to the total number of sites,

$$P_\infty = \frac{R_\parallel R_\perp^{(d_f - 1)}}{R_\parallel R_\perp^{(d-1)}} \tag{11}$$

for $R_\parallel < \xi_\parallel$ and $R_\perp < \xi_\perp$. Assuming $R_\parallel \sim \xi_\parallel$ and $R_\perp \sim \xi_\perp$, two hyperscaling relations could be obtained as

$$\nu_\perp(d_f - 1) + \nu_\parallel = \frac{1}{\sigma} \quad \text{and} \quad (d - 1)\nu_\perp - \beta = \nu_\perp(d_f - 1). \tag{12}$$

Eliminating d_f from the above relations another scaling relation could be obtained as

$$(d - 1)\nu_\perp + \nu_\parallel = \gamma + 2\beta = 2\delta - 3\gamma = 3\eta - 4\delta. \tag{13}$$

In the following, the values of the critical exponents will be determined and the scaling relations will be verified.

4 Results and discussions

Simulation is performed on a square lattice of size $2^{10} \times 2^{10}$. The critical probability p_c at which a spanning cluster appears for the first time in the system is determined first. The probability to have a spanning cluster is given by

$$P_{sp} = \frac{n_{sp}}{N_{tot}} = 1 - \sum_s {}' P_s(p) \tag{14}$$

where n_{sp} is the number of spanning clusters out of total $N_{tot} = 10^4$ number of clusters generated. In Figure 3, P_{sp} is plotted against the probability of occupation p. Note that, P_{sp} is not going to zero sharply at a particular value of p. This is due to the finite size of the lattice chosen here. The critical probability p_c is then determined from the maximum slope of the curve P_{sp} versus p. In the inset of Figure 3 the slope dP_{sp}/dp is plotted against p. It can be seen that the threshold p_c is at 0.655 ± 0.001 corresponding to the maximum slope. The derivative is calculated using
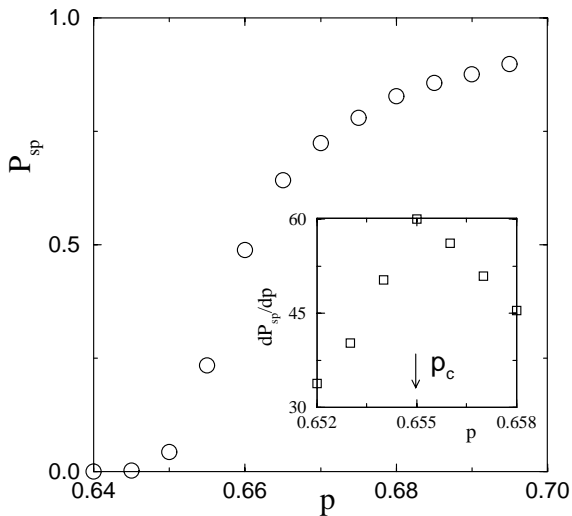
Fig. 3. Plot of spanning probability P_{sp} *versus* p (circles). In the inset the slope $\mathrm{d}P_{sp}/\mathrm{d}p$ is plotted against p (squares). The critical probability p_c is determined from the maximum slope and it is found $p_c = 0.655 \pm 0.001$ as indicated by an arrow.
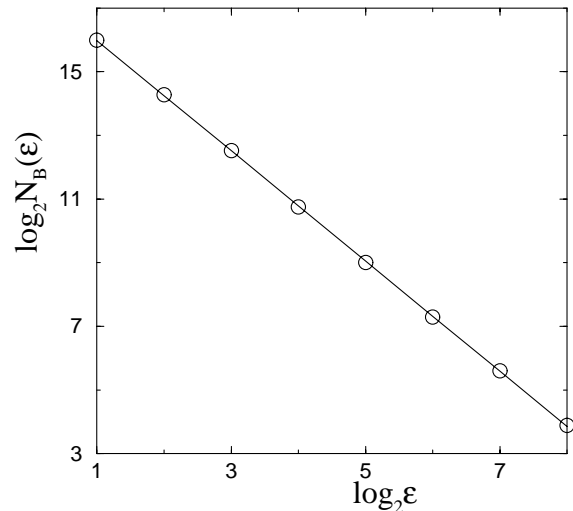

Fig. 4. Number of boxes $N_B(\epsilon)$ is plotted against the box size ϵ. Data are averaged over 512 samples. The fractal dimension is found $d_f = 1.733 \pm 0.005$.
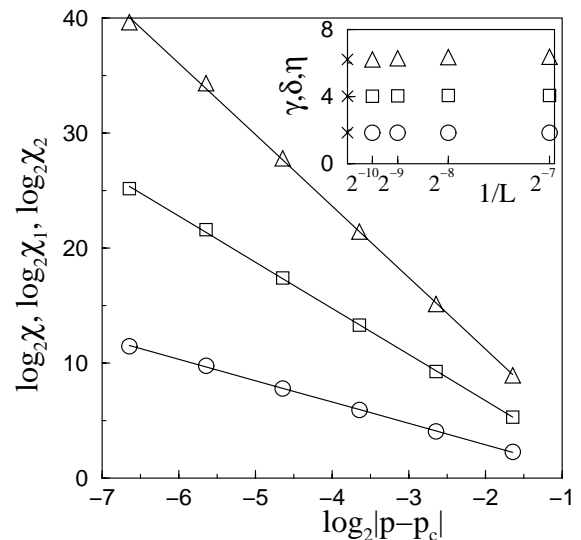

Fig. 5. Plot of the first, second and third moments χ, χ_1, and χ_2 of the cluster size distribution *versus* $|p - p_c|$. Different symbols are: circles for χ, squares for χ_1, and triangles for χ_2. The corresponding critical exponents are found as $\gamma = 1.85 \pm 0.01$, $\delta = 4.01 \pm 0.04$, and $\eta = 6.21 \pm 0.08$. In the inset, the values of the exponents γ ($\bigcirc$), δ ($\square$) and η ($\triangle$) are plotted against the system size $1/L$. Extrapolating to the infinite system size ($1/L = 0$), the values of the exponents obtained are $\gamma \approx 1.85$, $\delta \approx 4.01$, and $\eta \approx 6.21$.

the central difference method for the data points collected in an interval of 0.001. Note that, the value of p_c obtained here for the DSP model is slightly above the value of p_c of the directed percolation $p_c(DP) \approx 0.6445$ [16] and below the spiral percolation threshold $p_c(SP) \approx 0.712$ [17]. It is expected. Because, the rotational constraint tries to make the clusters compact by reoccupying the occupied sites of the directed clusters and, at the same time, the directional constraint tries to elongate the compact spiral clusters.

The infinite cluster, shown in Figure 2, generated on a 128×128 square lattice has holes of almost all possible sizes. It seems that the infinite clusters are self-similar and fractals. The fractal dimension d_f of the infinite clusters generated on the original $2^{10} \times 2^{10}$ lattice is determined by the box counting method. The number of boxes $N_B(\epsilon)$ is expected to vary with the box size ϵ as $N_B(\epsilon) \sim \epsilon^{d_f}$ where d_f is the fractal dimension. In Figure 4, $N_B(\epsilon)$ is plotted against the box size ϵ. The data are averaged over 512 samples. A reasonably good straight line is obtained in the log-log scale. The fractal dimension is found $d_f = 1.733 \pm 0.005$. The error is due to the least square fitting of the data points taking into account the statistical error of each point. The fractal dimension $d_f \approx 1.733$ ($\approx 12/7$) obtained here is the smallest among the fractal dimensions obtained in other percolation models. The values of d_f in other percolation models are: $d_f(OP) = 91/48$ [18], $d_f(DP) \approx 1.765$ [19], and $d_f(SP) \approx 1.957$ [17]. Also notice that the fractal dimension $d_f(DSP)$ obtained here is little higher than the fractal dimension 1.64 of ordinary lattice animals [20], large OP clusters below p_c. The infinite cluster generated in the DSP model is then the most rarefied one among the infinite clusters obtained in all four percolation models.

Next, the values of the critical exponents γ, δ, and η are estimated. The average cluster size χ and two other higher moments χ_1 and χ_2 are measured generating 10^4 finite clusters below p_c for six different p values. In Figure 5, χ, χ_1, and χ_2 are plotted against $|p - p_c|$. The circles represent χ, the squares represent χ_1 and the triangles represent χ_2. The values of the exponents obtained are $\gamma = 1.85 \pm 0.01$, $\delta = 4.01 \pm 0.04$, and $\eta = 6.21 \pm 0.08$. The errors quoted here are the standard least square fit error taking into account the statistical error of each single

Table 1. Comparison of the values of the critical exponents β, γ, τ, σ, ν, and d_f in the case of ordinary (OP), directed (DP), spiral (SP), and directed spiral (DSP) percolation on the square lattice. The values of the critical exponents of the DSP model are different from the other models. The values within parenthesis are the nearest rational fractions of the values of the critical exponents. These rational fractions satisfy the scaling relations exactly. The DSP model belongs to a new universality class.

Percolation Models	β	γ	τ	σ	ν	d_f
OP [18]	5/36	43/18	187/91	36/91	4/3	91/48
DP [19,21]	0.277 ± 0.002	2.2772 ± 0.0003	2.108 ± 0.001	0.3915 ± 0.0004	$\nu_\perp = 1.0972$ ± 0.0006 $\nu_\parallel = 1.733$ ± 0.001	1.765
SP [17]	0.048 ± 0.011	2.19 ± 0.07	2.022 ± 0.004	0.447 ± 0.014	1.116 ± 0.003	1.957 ± 0.009
DSP	0.31 ± 0.01 (1/3)	1.85 ± 0.01 (11/6)	2.16 ± 0.20 (28/13)	0.459 ± 0.004 (6/13)	$\nu_\perp = 1.12$ ± 0.03 (7/6) $\nu_\parallel = 1.33$ ± 0.01 (4/3)	1.733 ± 0.005 (12/7)

data point. The values of the exponents γ, δ, and η are also determined by the same Monte Carlo technique on the square lattices of three different smaller sizes $2^9 \times 2^9$, $2^8 \times 2^8$, and $2^7 \times 2^7$ to check the finite system size effects on the data. The values of the exponents γ (circles), δ (squares), and η (triangles) for different system sizes are plotted against the system size $1/L$ in the inset of Figure 5. It is then extrapolated upto $L \to \infty$, the infinite system size. The extrapolated values of the exponents are marked by crosses and the numerical values obtained are $\gamma \approx 1.85$, $\delta \approx 4.01$, and $\eta \approx 6.21$, the same as that of the system size $2^{10} \times 2^{10}$. These values of exponents are now used to verify the scaling relations obtained in Section 3. One of the scaling relations $\eta = 2\delta - \gamma$ obtained in equation (7) is checked now. The value of $2\delta - \gamma = 6.17$ is very close to the value of the exponent $\eta = 6.21$. The scaling relation $\eta = 2\delta - \gamma$ is then satisfied within error bars. Using the scaling relation $\delta = \beta + 2\gamma$ (Eq. (7)), the value of the exponent β is obtained as $\beta = 0.31 \pm 0.06$. The error has propagated from the errors of γ and δ. Independent estimation of the exponent β becomes difficult because of the presence of curvature in the plot of P_∞ versus $(p - p_c)$ in the log-log scale for $p > p_c$. This may be due to dominating corrections to scaling to the leading singularity of P_∞. The values of the exponents τ and σ can also be estimated using the scaling relations in equation (6). Three different values of τ could be obtained as $\tau_1 = (3\delta - 4\gamma)/(\delta - \gamma) = 2.14 \pm 0.18$, $\tau_2 = (4\eta - 5\delta)/(\eta - \delta) = 2.18 \pm 0.28$, and $\tau_3 = (3\eta - 5\gamma)/(\eta - \gamma) = 2.15 \pm 0.11$. The estimate of τ can be taken as the average of τ_1, τ_2 and τ_3 and it is given by $\tau = 2.16 \pm 0.20$. Similarly $\sigma = 0.459 \pm 0.015$ is determined from $\sigma_1 = 1/(\delta - \gamma) = 0.463 \pm 0.011$, $\sigma_2 = 1/(\eta - \delta) = 0.455 \pm 025$, and $\sigma_3 = 2/(\eta - \gamma) = 0.459 \pm 0.009$. The errors quoted here are the propagation errors. A comparison between the values of the exponents obtained in different percolation models is made in Table 1. It can be seen that the values of the exponents obtained in this model are very different from those obtained in other percolation

models like OP, DP, and SP. The magnitude of β is the largest and the magnitude of γ is the smallest among the four models. The DSP model then belongs to a new universality class. The values of the exponents obtained here could be approximated to the nearest rational fractions as $\beta \approx 1/3$, $\gamma \approx 11/6$, $\delta \approx 24/6$, $\eta \approx 37/6$, $\tau \approx 28/13$ and $\sigma \approx 6/13$. Surprisingly they satisfy all the scaling relations in equations (6, 7) exactly.

The connectivity lengths, $\xi_\parallel$ and $\xi_\perp$, for the system size $2^{10} \times 2^{10}$ are plotted against $|p - p_c|$ in Figure 6. The squares represent $\xi_\parallel$ and the circles represent $\xi_\perp$. The corresponding exponents $\nu_\parallel$ and $\nu_\perp$ are obtained as $\nu_\parallel = 1.33 \pm 0.01$ and $\nu_\perp = 1.12 \pm 0.03$. The errors quoted here are the least square fit errors. In the inset of Figure 6, $\nu_\parallel$ (squares) and $\nu_\perp$ (circles) are plotted against different system sizes $1/L$. The exponent values are extrapolated upto $L \to \infty$ and the extrapolated values are $\nu_\parallel \approx 1.33$ and $\nu_\perp \approx 1.12$, the same as obtained for the system size $2^{10} \times 2^{10}$. There are few things to notice. First, the value of $\nu_\parallel$ is almost equal to the connectivity exponent of ordinary percolation, $\nu(OP) = 4/3$ [18]. Recently, a study of magnetoresistance of a three-component composites consisting of cylindrical insulator and perfect conductors in a metallic host film is made by Barabash et al. [14]. Since the Hall effect will generate an electric field with a component perpendicular to the plane of the film with an in-plane applied current, their system appears inherently three dimensional (3D). However, the electric field perpendicular to the film plane vanishes because of the presence of columnar perfect conductor. Thus, their 3D problem reduces to that of calculating the effective conductivity of a 2D composites of perfect insulator and perfect conductor [3,14]. The results obtained in the model of composite material by Barabash et al. [14] then could be compared with the results of the present DSP model in 2 dimensions. It is found by Barabash et al. [14] that the correlation length exponent is 4/3 independent of anisotropy. The correlation length exponent quoted there is equivalent
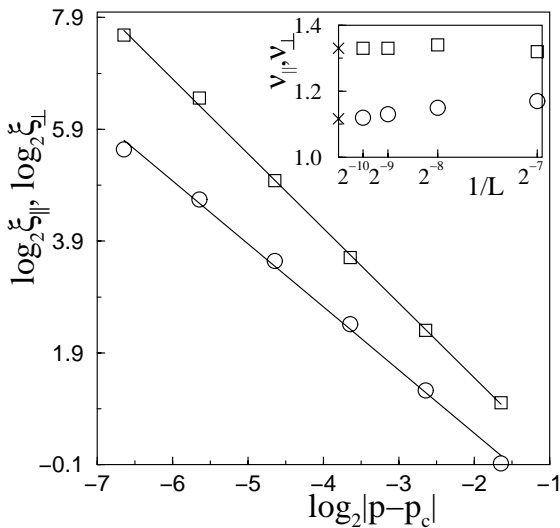
Fig. 6. The connectivity lengths, $\xi_\parallel$ and $\xi_\perp$, are plotted against $|p - p_c|$. The circles represent $\xi_\perp$ and the squares represent $\xi_\parallel$. The critical exponents are found as $\nu_\parallel = 1.33 \pm 0.01$ and $\nu_\perp = 1.12 \pm 0.03$. In the inset, the values of $\nu_\parallel$ ($\square$) and $\nu_\perp$ ($\bigcirc$) are plotted against the system size $1/L$. The values of the exponents are extrapolated upto $L \to \infty$. The extrapolated values of the exponents are marked by crosses and they are $\nu_\parallel \approx 1.33$ and $\nu_\perp \approx 1.12$.

to the connectivity exponent $\nu_\parallel$ of the DSP model considered here. The results of the DSP model is thus in good agreement with the results obtained in the model calculation of magnetoresistance of composite materials. Second, the values of $\nu_\parallel$ and $\nu_\perp$ are different from those obtained in the DP model, $\nu_\parallel(DP) = 1.733 \pm 0.001$ and $\nu_\perp(DP) = 1.0972 \pm 0.0006$ [21] (see Tab. 1 also). Third, the ratio of the connectivity lengths goes as $\xi_\parallel/\xi_\perp \sim |p - p_c|^{-\Delta\nu}$ where $\Delta\nu = \nu_\parallel - \nu_\perp$. In DSP, $\Delta\nu$ is approximately 0.21 whereas in DP, it is approximately 0.64. This means that clusters in the DSP model are less anisotropic than the clusters in the DP model at any p. This is due to the presence of the rotational constraint which tries to make the clusters isotropic. Barabash *et al.* [14] assumed that $\Delta\nu = 0$. The effective aspect ratio of their problem might vary as $|p - p_c|^{-\Delta\nu}$ with $\Delta\nu = 0.21$ as obtained here in the DSP model. Fourth, $(d - 1)\nu_\perp + \nu_\parallel$ is ≈ 2.45 for $d = 2$ and $2\delta - 3\gamma \approx 2.47$. The hyperscaling relation $2\delta - 3\gamma = (d - 1)\nu_\perp + \nu_\parallel$ in equation (13) is then satisfied within error bars. Two other hyperscaling relations $\nu_\perp(d_f - 1) + \nu_\parallel = 1/\sigma$ and $(d - 1)\nu_\perp - \beta = \nu_\perp(d_f - 1)$ given in equation (12) are also satisfied within error bars. In directed percolation hyperscaling is violated [22]. This is the first anisotropic percolation model where hyperscaling is satisfied. The values of the connectivity exponents $\nu_\parallel$ and $\nu_\perp$ could also be approximated to their nearest rational fractions as $\nu_\parallel \approx 4/3$ and $\nu_\perp \approx 7/6$. They satisfy the hyperscaling relations in equations (12, 13) exactly taking $d_f = 12/7$.

In the above study, it is found that the fractal dimension d_f and the values of the critical exponents (τ, σ, β, γ, $\nu_\parallel$, $\nu_\perp$, etc.) of DSP model are different from other

percolation models. As a consequence, the DSP model belongs to a new universality class. This is due to the fact that a completely new type of percolation cluster is generated in the DSP model. There are three important features of the DSP clusters. The clusters are rarefied, have spiraling danging ends, and are anisotropic. As the clusters grow, more and more vacancies are generated into the cluster. This is because, the clockwise rotational constraint tries to occupy sites away from the directional constraint whereas the directional constraint tries to occupy sites along itself in the x-direction. The effects of these two counter acting constraints are the following: the spiral clusters (clusters with spiraling dangling ends) become rarefied, become wider as it is away from the origin (see Fig. 2), and elongated along a clockwisely rotated direction from the original globally fixed directional constraint. The clusters are neither directed percolation clusters nor spiral percolation clusters. The combined directed and spiral constraints produces highly rarefied anisotropic spiral clusters. Individually, the effect of these three features, anisotrpoy [16], spiraling [17], and volume fraction [23], on the ordinary percolation clusters have been studied. Each of them corresponds to different critical behaviour and consequently belongs to new universality class. Here in DSP model, a new critical behaviour is obtained at the percolation threshold because of the presence of all three features in the same cluster.

Finally, the scaling function form assumed for the cluster size distribution $P_s(p) = s^{-\tau+1}\mathsf{f}[s^\sigma(p - p_c)]$ is verified. The scaled cluster size distribution $P_s(p)/P_s(p_c)$ is now plotted against the scaled variable $s^\sigma(p - p_c)$ in Figure 7. It is assumed that $\mathsf{f}[0]$ is a constant. The value of σ is taken as 0.459. Distribution of 10^4 clusters over the bins of width $2^{i-1} - (2^i - 1)$ with $i = 1$ to L^2 ($= 2^{20}$) is considered for each p value. In Figure 7, the cluster size s changes from 64 to 8192 and $(p - p_c)$ changes form 0.12 to -0.06. Data for different values of s and $(p - p_c)$ collapse reasonably onto a single curve. This means that the scaling function form assumed for the cluster size distribution is appropriate for this model. Also notice that the maximum value of $P_s(p)/P_s(p_c)$ for DSP model (≈ 3) is different from that of OP model (≈ 4.5) [4].

5 Conclusion

The new directed spiral site percolation, DSP model, under both directional and rotational constraints belongs to a new universality class. The combined directed and spiral constraints produces a new type of percolation clusters which are highly rarefied, anisotropic, and spiral in nature. The critical properties of the cluster related quantities in this model are very different from the other percolation models like OP, DP, and SP. The critical exponent γ of the average cluster size χ is the smallest and the exponent β of P_∞ is the largest among the four models. The fractal dimension $d_f \approx 12/7$ is the smallest among the four percolation models and thus the infinite clusters are highly rarefied here. Since the clusters generated in this model are anisotropic, two
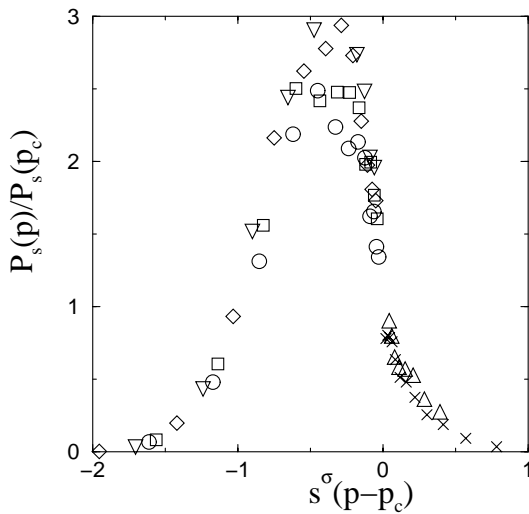
Fig. 7. Plot of the scaled cluster size distribution $P_s(p)/P_s(p_c)$ *versus* the scaled variable $s^\sigma(p - p_c)$ for different values of p with $\sigma = 0.459$. The cluster size s changes from 64 to 8192. The data plotted correspond to $p - p_c = 0.12$ ($\times$), 0.11 ($\triangle$), -0.03 ($\bigcirc$), -0.04 ($\square$), -0.05 ($\diamond$), and -0.06 ($\triangledown$). A reasonable data collapse is observed.

connectivity lengths, $\xi_\parallel$ and $\xi_\perp$, are defined to describe the scaling behaviour of the clusters connectivity as $p \rightarrow p_c$. The exponents $\nu_\parallel$ and $\nu_\perp$, associated with $\xi_\parallel$ and $\xi_\perp$, are estimated. The finite size effect on the exponent values is also checked making simulations on different system sizes and the values of the exponents are extrapolated to the infinite network. It is found that $\nu_\parallel$ is approximately equal to the connectivity exponent $\nu = 4/3$ of the OP model which is also in good agreement with the correlation length exponent ν obtained by Barabash *et al.* [14] in the study of magnetoresistance of a model composite material. Both $\nu_\parallel$ and $\nu_\perp$ are different from those obtained in the DP model. The order of anisotropy $\xi_\parallel/\xi_\perp$ is higher in the DP clusters than that of the clusters in the DSP model at any p. The critical exponents of the DSP model satisfy the scaling relations within error bars including the hyperscaling which is violated in the DP model. This is the first anisotropic percolation model where the hyperscaling is satisfied. The assumed scaling function form $P_s(p) = s^{-\tau+1}\mathrm{f}[s^\sigma(p - p_c)]$ of the cluster size distribution $P_s(p)$ is verified through data collapse. The values of all the critical exponents are suggested in terms of rational fractions and it is observed that those rational fractions satisfy the scaling relations exactly. The proposed rational fractions for the values of the critical exponents might be verified through an exact solution of the model. A difficulty in solving the model exactly is in the reoccupation of the same sites from different directions. The model will be applicable to the physical situations where both the directional and rotational constraints are present. For example, measurement

of magnetoresistance in composite materials, magnetic semiconductors, and super-ionic conductors could be studied using this model if it is extended to 3 dimensions. The model will also be applicable in studying the rheological properties of electro-rheological and magneto-rheological fluids in presence of crossed electric and magnetic fields.

References

1. M.V. Gandhi, B.S. Thompson, *Smart Materials and Structures* (Chapman and Hall, London, 1992)
2. H. Ohno, Science **281**, 951 (1998); G.A. Prinz, Science **282**, 1660 (1998)
3. D.J. Bergman, Y.M. Strelniker, Phys. Rev. B **59**, 2180 (1999); Phys. Rev. B **60**, 13016 (1999)
4. D. Stauffer, A. Aharony, *Introduction to Percolation Theory*, 2nd edn. (Taylor and Francis, London, 1994)
5. W. Kinzel, in *Percolation Structure and Processes*, edited by G. Deutscher, R. Zallen, J. Adler (Adam Hilger, Bristol, 1983)
6. P. Ray, I. Bose, J. Phys. A **21**, 555 (1988); S.B. Santra, I. Bose, J. Phys. A **24**, 2367 (1991)
7. S.P. Obukhov, Phys. Rev. Lett. **65**, 1395 (1990)
8. H. Hinrichsen, Adv. Phys. **49**, 815 (2000)
9. O. Stenull, H.-K. Janssen, Phys. Rev. E **64**, 016135 (2001) and references therein
10. S.B. Santra, I. Bose, Z. Phys. B **89**, 247 (1992)
11. S.B. Santra, A. Paterson, S. Roux, Phys. Rev. E **53**, 3867 (1996)
12. S.B. Santra, W.A. Seitz, Int. J. Mod. Phys. C **11**, 1357 (2000) and references therein
13. A. Bunde, S. Havlin, in *Fractals and Disordered Systems*, edited by A. Bunde, S. Havlin (Springer-Verlag, Berlin, 1991)
14. S.V. Barabash, D.J. Bergman, D. Stroud, Phys. Rev. B **64**, 174419 (2001)
15. P.L. Leath, Phys Rev. B **14**, 5046 (1976)
16. D. Dhar, M. Barma, J.Phys. C **14**, L1 (1981)
17. S.B. Santra, I. Bose, J. Phys. A **25**, 1105 (1992)
18. M.P.M. den Nijs, J. Phys. A **12**, 1857 (1997); B. Nienhuis, J. Phys. A **15**, 199 (1982)
19. B. Hede, J. Kertész, T. Vicsek, J. Stat. Phys. **64**, 829 (1991)
20. T.C. Lubensky, J. Isaacson, Phys. Rev. Lett. **46**, 871 (1981)
21. J.W. Essam, K. DéBell, J. Adler, Phys. Rev. B **33**, 1982 (1986); J.W. Essam, A.J. Guttmann, K. DéBell, J. Phys. A **21**, 3815 (1988)
22. M. Henkel, V. Privman, Phys. Rev. Lett. **65**, 1777 (1990)
23. J. Kertész, J. Phys. France **42**, L393 (1981)